REVISED

CONF-820434--19

# A POSITRON-ANNIHILATION STUDY OF THE EQUILIBRIUM VACANCY ENSEMBLE IN ALUMINUM*

CONF-820434--19

DE83 007623

M. J. Fluss‡†, S. Berko‡, B. Chakraborty†, K. Hoffmann‡, P. Lippel ‡, and R. W. Siegel†

‡Department of Physics, Brandeis University
Waltham, Massachusetts 02254, USA
†Materials Science Division, Argonne National Laboratory
Argonne, Illinois 60439, USA



JUNE 1982



*This work was supported by the U.S. Department of Energy and National Science Foundation.

Submitted to the Sixth International Conference on Positron Annihilation, Fort Worth, Texas, 3-7 April 1982.

# A POSITRON-ANNIHILATION STUDY OF THE EQUILIBRIUM VACANCY ENSEMBLE IN ALUMINUM*

M. J. Fluss‡†, S. Berko‡, B. Chakraborty†, K. Hoffmann‡, P. Lippel‡, and R. W. Siegel†

‡Department of Physics, Brandeis University
Waltham, Massachusetts 02254, USA
†Materials Science Division, Argonne National Laboratory
Argonne, Illinois 60439, USA

A preliminary report is presented of a positron-annihilation study of the equilibrium vacancy ensemble in aluminum using one- and two-dimensional angular correlation of annihilation radiation (ACAR) measurements versus temperature. The annihilation characteristics of a positron from the Bloch state, and the monovacancy- and divacancy-trapped states have been calculated self-consistently within a supercell, including many-body enhancement effects, and are compared with experiment.

## 1. INTRODUCTION

Positron annihilation experiments can yield valuable information about vacancy defects in metals [1]. Aluminum was chosen for the present study, since it is accessible experimentally and theoretically and can serve as a model material for equilibrium vacancy-ensemble studies: it has a relatively large vacancy concentration at melting [$C_v(T_m) \sim 10^{-3}$], and thus a wide temperature range (~200°C) in which over 90% of positrons annihilate from vacancy-trapped states. Also, Al is expected to have [2] a significant concentration of divacancies in its high-temperature equilibrium ensemble [$C_{2v}(T_m) \approx 0.2\ C_v(T_m)$]; it should therefore be possible to observe changes in the nature of the defect ensemble with increasing temperature by positron annihilation. In this preliminary report, results are discussed regarding the electron momentum density as sampled by the positron as a function of temperature, using the two-dimensional angular correlation of annihilation radiation (2D-ACAR) technique [3]. Data from single-crystal Al at 500°C and 630°C, where positron trapping dominates, are compared with data from 20°C, where positrons annihilate from delocalized Bloch states. A complete set of long-slit (1D-ACAR) results have also been obtained, as well as 2D-ACAR data at 340°C and 575°C; these will be presented in a fuller account of this investigation.

## 2. EXPERIMENT

The present experiments were performed at Brandeis University with the "triple-counter pair" long-slit (1D-ACAR) apparatus, and the multi-counter cross-correlation 2D-ACAR instrument [3]. Aluminum single crystals were mounted on a stainless steel, resistively-heated block, which was inserted into a UHV ($10^{-7}$ to $10^{-8}$ Torr) chamber positioned between the pole faces of a positron-focusing magnet. Temperatures were measured with chromel-alumel thermocouples held between the Al sample and the heating block. Temperature stability was maintained either manually (to ± 5°C) or by a feedback system (to ± 1°C). At 630°C, the temperature could have been underestimated by as much as ~10°C. The positron "spot size" on the 10 mm diameter samples was ~6 mm in diameter; hence significant temperature gradients over the sampled area were unlikely. The samples were annealed in situ at 630°C. Peak-counting and full long-slit 1D-ACAR measurements versus temperature were performed for three crystal orientations, <100>, <110>, and <111>. One of the three independent long-slit pair detectors was set at 2.0 mrad FWHM, and the others at 0.5 mrad FWHM resolution. The 2D-ACAR data at temperature T, $N_T(p_y,p_z)$, were obtained for a <100> axis along the integration direction $p_x$, and <110> axes along $p_y$ and $p_z$. Lead collimators with 1.5 cm diameter circular holes in front of each of the 64 NaI detectors (at 10 m from the sample-source assembly) were used. Positrons were obtained from 100-300 mCi $^{58}Co$ sources.

## 3. THEORY

The positron annihilation characteristics in a monovacancy and a divacancy were calculated using a self-consistent pseudopotential scheme, based upon a local density functional formalism incorporating many-body enhancement effects [4]. Application of this formalism to defect-free Al now yields results [5] in good agreement with the earlier, high-resolution, low-temperature 2D-ACAR measurements from Brandeis [6] on Al. The environment of the vacancies was simulated by an unrelaxed 27-atomic-site supercell to which the band-structure scheme was then applied [7,8]. The electronic structures of the monovacancy [7,8] and the divacancy [8], in the absence of the positron, have been calculated previously using this scheme. It was shown that the electronic structure of the monovacancies are effectively isolated in this supercell; the electronic structure of the divacancy is not so immune to supercell effects. However, in both the monovacancy- and divacancy-trapped positron states, the positron is extremely well localized; the perturbation from neighboring defects

is therefore too small to significantly affect the electronic structure as seen by the positron, and hence the present theoretical results are expected to be independent of supercell configuration. Owing to crystal symmetry, a six-fold spatial average must be performed for the divacancy results before comparison with experiment can be made. The ACAR spectra for the two defect-trapped states were determined following the method of Refs. [4] and [5].

## 4. RESULTS AND DISCUSSION

Figure 1 shows the experimental $N_T(p_y,p_z)$ surfaces in a semi-logarithmic format, at 20°C, 500°C, and 630°C. The Umklapp peaks in the high-momentum regions are clearly visible at 20°C, even with the low-resolution collimators used here, and agree well with the previous high-resolution data [3,6]. Some lower intensity high-momentum anisotropy is also present in the high temperature data. Figure 2 shows the results of the theoretical calculations for the 2D-ACAR surfaces for the Bloch, the monovacancy- and the divacancy-trapped positron states at 0°K, $N_{Bloch}$, $N_{1v}$, and $N_{2v}$, respectively. The theoretical results are all normalized to the same volume; the $N_{Bloch}(p_y,p_z)$ is normalized to the peak of the experimental $N_{20}(p_y,p_z)$ data. The $p_z$ and $p_y$ axes in Fig. 2 correspond to <100> directions (the <110> directions are the diagonals); the perspective drawings have been rotated so as to coincide with the experimental orientations. The appropriate resolution has been included in these theoretical results. A comparison of Figs. 1 and 2 shows that (i) he Bloch-state theory fits the 20°C spectrum rather well, except for the magnitude of the Umklapp peaks, which are underestimated because of the pseudopotential approach used, and (ii) the shapes of the experimental 500°C and 630°C surfaces both lie between the calculated monovacancy and divacancy surfaces, with peak heights increasing in the order $N_{1v}$, $N_{500}$, $N_{630}$, $N_{2v}$.

In order to determine if the theory can adequately describe the main features of the observed temperature dependence, first it was necessary to subtract from the $N_{500}$ and $N_{630}$ data the fraction of the $N_{20}$ data corresponding to the percentage of positrons still annihilating from Bloch states at these high temperatures (no correction was made to account for the change in the Bloch state from 20°C to 500°C and 630°C). The Bloch-state fractions (6% at 500°C and 1% at 630°C) were obtained, to first-order, by analyzing the long-slit data using the two-state trapping model [1]. The high-temperature trapped-state surfaces $N'_{500} = C_{500}(N_{500} - 0.06N_{20})$ and $N'_{630} = C_{630}[N_{630} - 0.01N_{20}]$ were thus formed, where $C_{500}$ and $C_{630}$ are volume renormalization constants to match the volume of $N_{20}$. Difference surfaces between the various states of the positron could then be constructed for both experiment and theory. The difference surface $N'_{500} - N_{20}$ is shown in Fig. 3a; the <110>

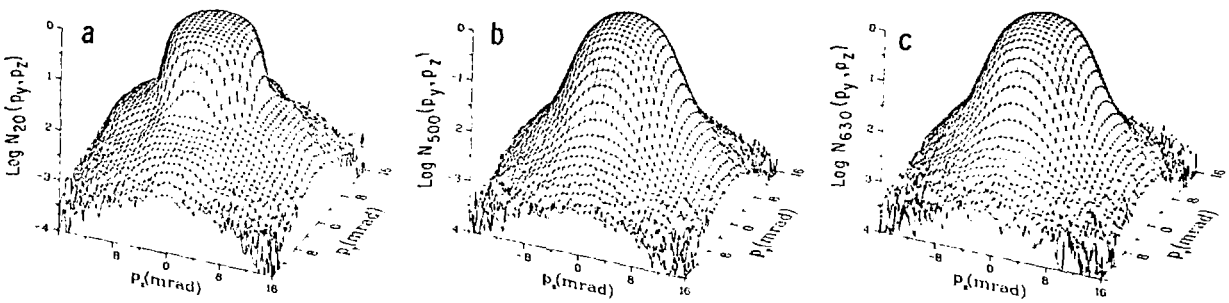


Fig. 1. Perspective representations of the experimental 2D-ACAR data for an Al single crystal at (a) 20°C, (b) 500°C, and (c) 630°C; the momentum axes $p_z$ and $p_y$ correspond to <110> directions.

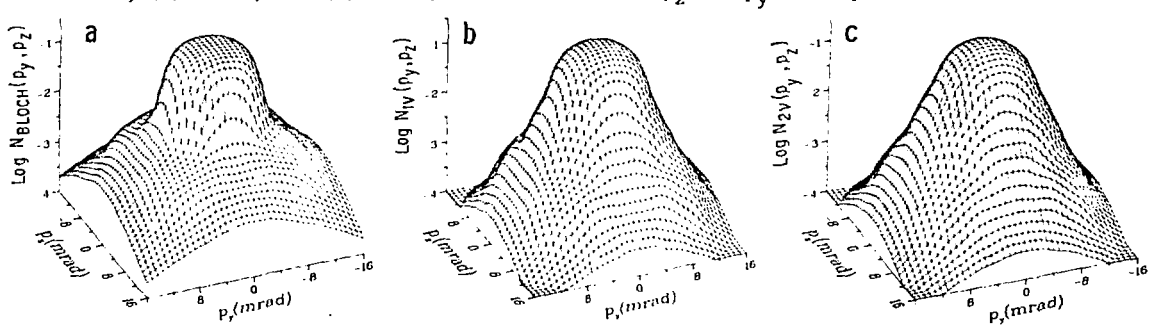


Fig. 2. Perspective representations of the calculated 2D-ACAR surfaces at 0°K, convoluted with the experimental resolution, for (a) the Bloch state and the (b) monovacancy- and (c) divacancy-trapped states of the positron. The axes $p_z$ and $p_y$ correspond to <100> directions.

Fig. 3. Difference surfaces for the 2D-ACAR data and <110> radial cuts through 8-fold symmetrized versions of these difference surfaces. Experiment: (a) $N'_{500}-N_{20}$, positron trapped-state data at 500°C minus the Bloch-state data at 20°C, and (b) $N'_{630}-N_{20}$ and $N'_{500}-N_{20}$, in units of percent of $N_{20}(p_z = 0, p_y = 0)$. Theory: (c) $N_{1v}-N_{Bloch}$, monovacancy-trapped state minus Bloch-state at 0°K, and (d) $N_{2v}-N_{Bloch}$ and $N_{1v}-N_{Bloch}$ at 0°K, in units of percent of $N_{Bloch}(p_z = 0, p_y = 0)$.

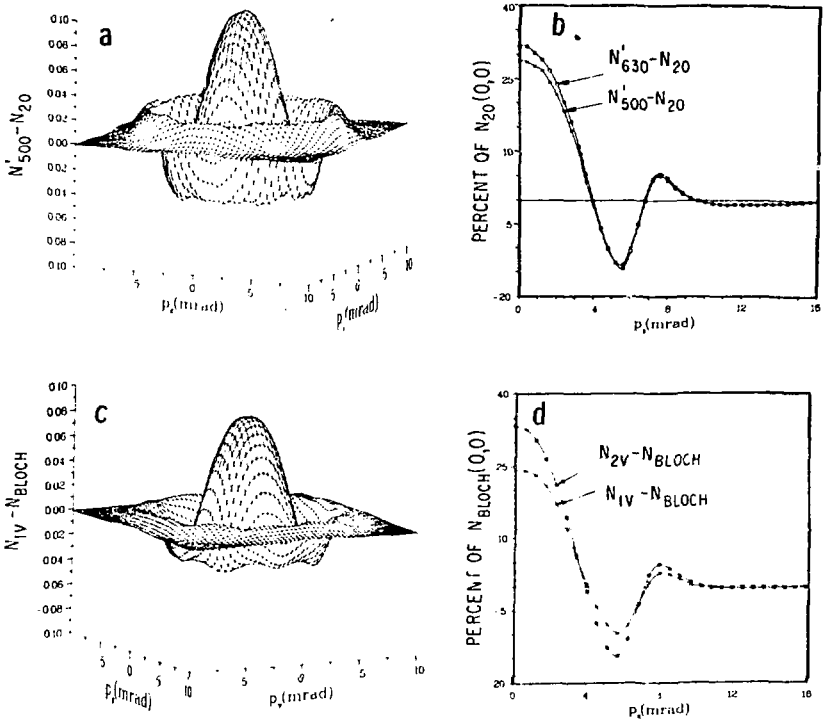


Fig. 4. Difference surfaces for the 2D-ACAR data and <110> radial cuts through 8-fold symmetrized versions of these difference surfaces. Experiment: (a) $N'_{630}-N'_{500}$, positron trapped-state data at 630°C minus those at 500°C; the upper data show the statistical scatter in forming this difference; the lower surface is smoothed with a Gaussian of $\sigma$ = 1.5 mrad, and (b) $N'_{630}-N'_{500}$ and $N'_{575}-N'_{500}$, in units of percent of $N_{500}(p_z = 0, p_y = 0)$. Theory: (c) $N_{2v}-N_{1v}$, divacancy-trapped state minus monovacancy-trapped state at 0°K, and (d) $N_{2v}-N_{1v}$ at 0°K, in units of percent of $N_{1v}(p_z = 0, p_y = 0)$.

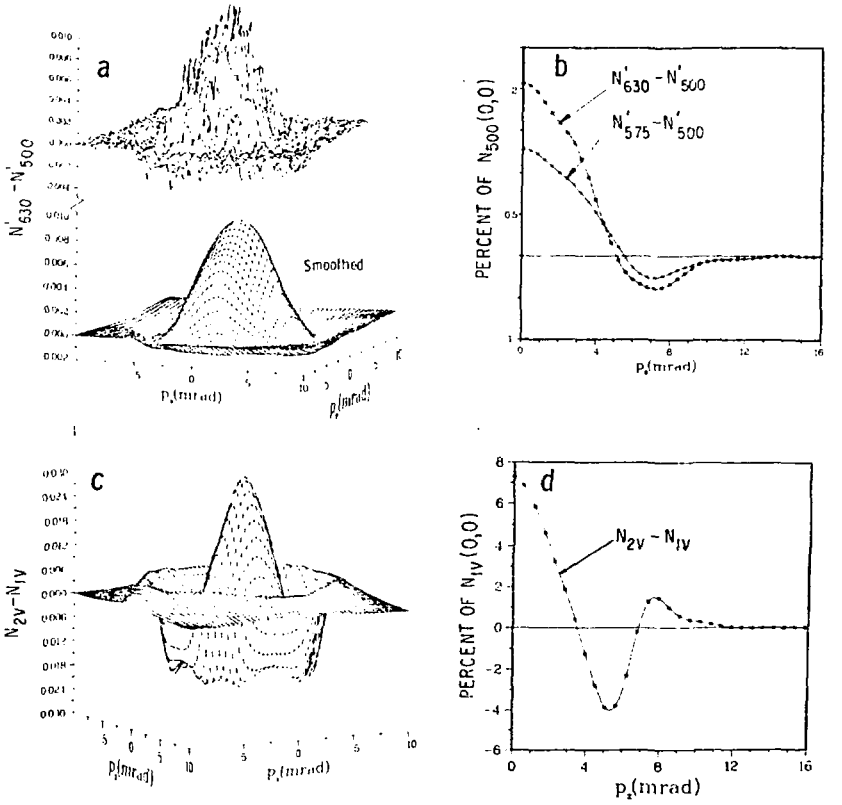

radial cuts for $N'_{630}-N_{20}$ and $N'_{500}-N_{20}$ are shown in Fig. 3b. For comparison, the theoretical $N_{1v}-N_{Bloch}$ surface and the corresponding radial cuts for $N_{2v}-N_{Bloch}$ and $N_{1v}-N_{Bloch}$ are presented in Figs. 3c and 3d. The major qualitative features, for both the experiment and theory, are the multiple maxima and multiple crossings of the nodal plane. Analogous observations using 1D-ACAR have been reported previously [9,10], and modeled [9] using a modified Wigner-Seitz method. The shape of the theoretical $N_{1v}-N_{Bloch}$ surface follows rather well the shapes of the experimental $N'_{500}-N_{20}$ and $N'_{630}-N_{20}$ surfaces. The absolute magnitude of this theoretical difference accounts for ~90% of the experimentally observed $N'_{500}-N_{20}$ at its peak, and ~80% of the $N'_{630}-N_{20}$ difference. The positive and negative ridges at higher momenta are also underestimated. Such a result is encouraging, since it supports the idea of an expected significant and increasing divacancy contribution with increasing temperature. However, a precise quantitative comparison must await further work, as indicated by a more detailed comparison between the high-temperature trapped-state data.

The effect of changing the temperature from 500°C to 630°C can be further investigated by a comparison of the difference surface $N'_{630}-N'_{500}$, shown in Fig. 4a, and the theoretical $N_{2v}-N_{1v}$ surface shown in Fig. 4c. The corresponding <110> radial cuts for these surfaces, and $N'_{575}-N'_{500}$, are shown in Figs. 4b and 4d. The effect of static lattice expansion from 500°C to 630°C on $N_{1v}$ has been calculated, and found to be negligible with respect to the ~20 times larger experimental effect shown in Figs. 4a and 4b. The theoretical $N_{2v}-N_{1v}$ shows, on the other hand, a large effect at the peak. This suggests that a significant and increasing fraction of positrons trapped at divacancies could explain the observed peak-height changes between 500°C and 630°C. However, in the absence of any other temperature effects, the difference surfaces $N'_{630}-N'_{500}$ and $N_{2v}-N_{1v}$ should be equal within a multiplication factor (Fig. 4c would be suppressed by a factor <1, which depends on the relative trapping at divacancies between 630°C and 500°C). The shape of $N'_{630}-N'_{500}$ is, however, distinctly different from the theoretical shape of $N_{2v}-N_{1v}$. Thus, before the presence of divacancies can be verified, other temperature-dependent effects have to be taken into account in the theory.

Among the temperature-dependent effects still to be taken into account are: (i) static lattice expansion for the divacancy state, (ii) lattice expansion and phonon coupling in the Bloch state, and (iii) the effects of the local atomic vibrations around the vacancy and divacancy. The thermal smearing effects, both from the positron and the atoms, are expected to suppress the various theoretically predicted peak-height differences. In addition, the lattice (atomic) relaxations around the vacancy defects in the presence of the trapped positron must be taken into account. Preliminary calculations, using the present formalism, have shown that the trapped positron exerts an outward pressure on the first-nearest-neighbor atoms around the monovacancy, as previously suggested [11]. A similar effect might be expected for the divacancy. Work is in progress on these various effects. The observed anisotropies of the 2D-ACAR data will be more carefully studied for indications of the changing nature of the defect ensemble. It is anticipated that further analysis of the 2D-ACAR data with a theoretical model incorporating additional temperature-dependent effects will yield valuable information regarding the presence of divacancies in the equilibrium vacancy ensemble in aluminum.

We thank F. Sinclair for many valuable discussions and suggestions regarding this study. One of us (MJF) wishes to acknowledge the hospitality of the Physics Department of Brandeis University during 1980-1981.

*This work was supported by the U.S. Department of Energy under contract No. W-31-109-ENG-38 and NSF Grant DMR-7926035.

REFERENCES

[1] Siegel, R. W., Scripta Metall. 14 (1980) 15; for various applications see Positrons in Solids, Hautojarvi, P., eds. (Springer-Verlag, Berlin, 1979) pp. 255.

[2] Siegel, R. W., J. Nucl. Mater. 69 & 70 (1978) 117.

[3] Berko, S., Haghgooie, M., and Mader, J. J., Phys. Lett. 63A (1977) 335; for details about the apparatus, see Berko, S., in Positron Annihilation, Hasiguti, R. R., and Fujiwara, K., eds. (Japan Institute of Metals, Sendai, 1979) p. 65.

[4] Chakraborty, B., Phys. Rev. B 24 (1981) 7423.

[5] Chakraborty, B., these Proceedings.

[6] Mader, J., Berko, S., Krakauer, H., and Bansil, A., Phys. Rev. Lett. 37 (1976) 1232.

[7] Chakraborty, B., Siegel, R. W., and Pickett, W. E., Phys. Rev. B 24 (1981) 5445.

[8] Chakraborty, B. and Siegel, R. W., Proc. Yamada Conf. V on Point Defects and Defect Interactions in Metals, Kyoto 1981, Takamura, J., et al., eds. (University of Tokyo Press, 1982) in press.

[9] Shulman, M. A. and Berko, S., Proc. Fourth Intl. Conf. on Positron Annihilation, Helsingør, Denmark 1976, paper E31, unpublished; Shulman, M. A., Ph. D. Thesis, Brandeis University (1980).

[10] Triftshäuser, W, Phys. Rev. B 12 (1975) 4634.

[11] Tam, S. W. and Siegel, R. W., J. Phys. F: Metal Phys. 7 (1977) 877.